DIGITAL ACCESS TO SCHOLARSHIP AT HARVARD
DASH.HARVARD.EDU

HARVARD LIBRARY
Office for Scholarly Communication

Climate response to the increase in tropospheric ozone since preindustrial times: A comparison between ozone and equivalent CO 2 forcings

Citation
Mickley, L. J., D. J. Jacob, B. D. Field, and D. Rind. 2004. "Climate Response to the Increase in Tropospheric Ozone Since Preindustrial Times: A Comparison Between Ozone and Equivalent CO2 Forcings." Journal of Geophysical Research 109 (D5). doi:10.1029/2003jd003653.

Published Version
doi:10.1029/2003JD003653

Permanent link
http://nrs.harvard.edu/urn-3:HUL.InstRepos:14121783

Terms of Use
This article was downloaded from Harvard University's DASH repository, and is made available under the terms and conditions applicable to Other Posted Material, as set forth at http://nrs.harvard.edu/urn-3:HUL.InstRepos:dash.current.terms-of-use#LAA

Share Your Story

The Harvard community has made this article openly available.
Please share how this access benefits you. Submit a story .

Accessibility

Climate response to the increase in tropospheric ozone since preindustrial times: A comparison between ozone and equivalent CO_2 forcings

L. J. Mickley, D. J. Jacob, and B. D. Field
Division of Engineering and Applied Sciences, Harvard University, Cambridge, Massachusetts, USA

D. Rind
Goddard Institute for Space Studies, Columbia University, New York, USA

Received 1 April 2003; revised 6 October 2003; accepted 6 November 2003; published 11 March 2004.

[1] We examine the characteristics of the climate response to anthropogenic changes in tropospheric ozone. Using a general circulation model, we have carried out a pair of equilibrium climate simulations with realistic present-day and preindustrial ozone distributions. We find that the instantaneous radiative forcing of 0.49 W m^{-2} due to the increase in tropospheric ozone since preindustrial times results in an increase in global mean surface temperature of 0.28°C. The increase is nearly 0.4°C in the Northern Hemisphere and about 0.2°C in the Southern Hemisphere. The largest increases (>0.8°C) are downwind of Europe and Asia and over the North American interior in summer. In the lower stratosphere, global mean temperatures decrease by about 0.2°C due to the diminished upward flux of radiation at 9.6 μm. The largest stratospheric cooling, up to 1.0°C, occurs over high northern latitudes in winter, with possibly important implications for the formation of polar stratospheric clouds. To identify the characteristics of climate forcing unique to tropospheric ozone, we have conducted two additional climate equilibrium simulations: one in which preindustrial tropospheric ozone concentrations were increased everywhere by 18 ppb, producing the same global radiative forcing as present-day ozone but without the heterogeneity; and one in which CO_2 was decreased by 25 ppm relative to present day, with ozone at present-day values, to again produce the same global radiative forcing but with the spectral signature of CO_2 rather than ozone. In the first simulation (uniform increase of ozone), the global mean surface temperature increases by 0.25°C, with an interhemispheric difference of only 0.03°C, as compared with nearly 0.2°C for the heterogeneous ozone increase. In the second simulation (equivalent CO_2), the global mean surface temperature increases by 0.36°C, 30% higher than the increase from tropospheric ozone. The stronger surface warming from CO_2 is in part because CO_2 forcing (obscured by water vapor) is shifted relatively poleward where the positive ice-albedo feedback amplifies the climate response and in part because the magnitude of the CO_2 forcing in the midtroposphere is double that of ozone. However, we find that CO_2 is far less effective than tropospheric ozone in driving lower stratospheric cooling at high northern latitudes in winter. *INDEX TERMS:* 0340 Atmospheric Composition and Structure: Middle atmosphere—composition and chemistry; 0345 Atmospheric Composition and Structure: Pollution—urban and regional (0305); 0365 Atmospheric Composition and Structure: Troposphere—composition and chemistry; 1610 Global Change: Atmosphere (0315, 0325); *KEYWORDS:* tropospheric ozone, climate change, stratospheric ozone

Citation: Mickley, L. J., D. J. Jacob, B. D. Field, and D. H. Rind (2004), Climate response to the increase in tropospheric ozone since preindustrial times: A comparison between ozone and equivalent CO_2 forcings, *J. Geophys. Res.*, *109*, D05106, doi:10.1029/2003JD003653.

1. Introduction

[2] Radiative forcing is typically defined as the radiative flux imbalance at the tropopause that occurs when a perturbation is applied to the atmosphere. It is commonly used as a metric to determine the relative importance of different greenhouse gases and aerosols to climate. For example, the Intergovernmental Panel on Climate Change (IPCC) reports global and annual mean radiative forcings since preindustrial times of 1.4 W m^{-2} for CO_2, −0.5 to −0.9 W m^{-2} for sulfate aerosols (direct effect), and 0.3 to

Copyright 2004 by the American Geophysical Union.
0148-0227/04/2003JD003653$09.00

0.5 W m^{-2} for tropospheric ozone [*Houghton et al.*, 2001]. The radiative forcing by tropospheric ozone is assigned a ''medium'' level of scientific understanding by IPCC [*Houghton et al.*, 2001], although we have contended that our understanding is less due to the difficulty of constraining preindustrial levels of ozone [*Mickley et al.*, 2001]. Aside from this issue, comparison of radiative forcings averaged over the year and the globe may not adequately describe the regional climate response for short-lived species, such as tropospheric ozone and aerosols, whose forcings are highly heterogeneous. While local feedback mechanisms determine much of the surface temperature response to a particular forcing [*Boer and Yu*, 2003], the pattern of forcing can also influence the response [*Williams et al.*, 2001; *Boer and Yu*, 2003; *Joshi et al.*, 2003]. In addition, radiative forcing, as usually reported, overlooks the wavelength dependence of the flux perturbation (e.g., shortwave versus longwave), which could influence heating and cooling rates in the atmosphere. We use here a general circulation model to diagnose the unique climate response from radiative forcing by tropospheric ozone and compare it in particular to the climate response to an equivalent CO_2 global forcing.

[3] Ozone is produced in the troposphere by photochemical oxidation of volatile organic compounds (VOCs) and CO in the presence of nitrogen oxides (NOx = NO + NO_2). Anthropogenic activities provide large global sources of VOCs, CO, and NO_x, driving the increase of tropospheric ozone since preindustrial times. The lifetime of ozone in the troposphere is typically a few weeks [*Wang and Jacob*, 1998], so there are large spatial and seasonal gradients that affect the radiative forcing. *Mickley et al.* [1999] found forcings greater than 1.2 W m^{-2} at high northern latitudes in summer. The longwave forcing by ozone is mainly due to absorption in the 9.6 μm window, where absorption by water vapor is weak. It is therefore less sensitive to local humidity than the forcing by CO_2 and CH_4, for which there is much more overlap with the H_2O absorption bands [*Lenoble*, 1993]. Finally, unlike other major greenhouse gases, ozone absorbs the solar wavelengths that penetrate to the troposphere. This shortwave forcing due to ozone is especially important over the poles, where the albedo of snow and ice is high and ozone may intercept reflected as well as incident sunlight [*Mickley et al.*, 1999].

[4] The short chemical lifetime of ozone means that its forcing responds rapidly to changes in emissions of ozone precursors. Because ozone not only contributes to climate change but also is a pernicious air pollutant toxic to humans and vegetation, imposing controls on precursor emissions promises multiple benefits [*Hansen et al.*, 2000; *Hansen and Sato*, 2001]. Identifying the consequences to climate that are specific to an ozone forcing will help in the evaluation of proposals to mitigate climate change through emissions controls.

[5] In most previous work investigating climate response to tropospheric ozone, idealized or uniform ozone changes were employed. For example, *Ramaswamy and Bowen* [1994] applied the observed stratospheric ozone losses through the mid-1980s together with a uniform 20% increase in tropospheric ozone to a one-dimensional radiative-convective model. They found that the tropospheric ozone increase enhanced the cooling at 20 km due to stratospheric ozone loss by about one-fourth. Using perpetual January conditions and fixed sea ice coverage in a GCM and multiplying climatological tropospheric ozone fields by factors of 0.5 and 10, *Christiansen* [1999] calculated a climate sensitivity similar to that of a doubled CO_2 simulation. *Stuber et al.* [2001] also found that uniform increases of ozone to the middle and lower troposphere yielded a similar temperature response as an equivalent forcing of CO_2. Both *Stuber et al.* [2001] and *Joshi et al.* [2003], however, found that uniform increases of ozone to the upper troposphere generated a weaker surface temperature response than an equivalent forcing by CO_2. Finally, *Hansen et al.* [1997] found that cloud feedbacks in a GCM amplified the surface temperature response to ozone increases in the middle to lower troposphere.

[6] Two studies have applied more realistic tropospheric ozone increases to a radiation model or GCM to calculate the climate response. Using the fixed dynamical heating (FDH) approximation and the calculated ozone increase since preindustrial times, *Berntsen et al.* [1997] found a 0.2–0.4°C cooling in much of the lower stratosphere. *Hansen et al.* [2002], attempting to simulate the observed temperature rise since preindustrial times, included the rise in tropospheric ozone as one of a suite of changes in greenhouse gas and aerosol concentrations over that time period.

[7] Finally, a few model studies have examined the climate impact of the heterogeneous forcing due to aerosol. For example, *Menon et al.* [2002] found that black carbon emissions over southern China increase drought in northern China. *Chung et al.* [2002], on the other hand, calculated that Asian haze leads to increased rainfall in India during the dry monsoon season. *Williams et al.* [2001] calculated Northern Hemisphere cooling and a southward shift in the inter-tropical convergence zone (ITCZ) in response to the indirect effects of increasing anthropogenic sulfate aerosol.

[8] In our work, we diagnose the particularities in the climate response to a realistic change in tropospheric ozone with accompanying cloud feedbacks. We use a global circulation model (GCM) to first calculate the change in tropospheric ozone from preindustrial times to the present day and then to examine the climate response to this change, taking into account the inhomogeneous distribution of ozone. The magnitude of the response generated by this study should be considered a lower limit, since our model as well as others overestimates preindustrial ozone compared to existing 19th century observations [*Mickley et al.*, 2001]. To gauge the significance of the inhomogeneity of the ozone forcing, we also calculate the climate response to an increase in ozone mixing ratio uniformly applied throughout the troposphere. To diagnose the effect of the wavelength dependence of the ozone forcing, we calculate the climate response to a global increase in CO_2 that yields the same forcing as the ozone increase.

[9] Section 2 of this paper describes the model simulations. In section 3 we present the results of the simulations, and in section 4 we discuss our conclusions.

2. Model Description

[10] We use the GISS GCM 2′ of *Rind and Lerner* [1996] and *Rind et al.* [1999] with a ''qflux'' ocean [*Hansen et al.*,

1988]. The GISS model has been used extensively to probe the climate response to perturbations in greenhouse gas concentrations, solar luminosity, and tropospheric aerosol burden [e.g., *Hansen et al.*, 1997, 2002; *Rind et al.*, 2001; *Shindell et al.*, 2001a, 2001b; *Menon et al.*, 2002]. The version we use has a horizontal resolution of 4° latitude and 5° longitude, with nine vertical layers in a sigma coordinate system extending from the surface to 10 hPa. In the qflux ocean model, monthly mean ocean heat transport fluxes are first calculated to generate observed, present-day sea surface temperatures. In subsequent simulations, the sea surface temperatures and ocean ice respond to changes in climate, but the ocean heat transport fluxes are held fixed. While the qflux model cannot simulate the reduction in North Atlantic deep water formation predicted for a warming climate [*Russell and Rind*, 1999], previous work has shown that the assumption of zero interaction between ocean heat transport and climate change is acceptable for small perturbations such as those applied here [*Manabe and Bryan*, 1985]. To avoid runaway freezing of the Southern Hemisphere oceans, we have specified the ocean ice albedo at the low value of 0.25. (To achieve a reasonable ocean ice cover, other versions of the GISS GCM have also employed reduced ocean ice albedos [e.g., *Hansen et al.*, 1997].) This will have implications for the climate change experiments, which we will address in the Discussion section. The model relies on the correlated *k*-distribution method in calculating the radiative flux through the atmosphere [*Hansen et al.*, 1983]. In this method, the absorption coefficients are reordered, resulting in a smooth dependence of absorption coefficient versus artificial wavenumber. In the solar part of spectrum, the model uses 12 *k* profiles for multiple scattering: 5 for H_2O, 3 for CO_2, 3 for ozone, and 1 for NO_2. Absorption of the direct beam is calculated separatedly for H_2O, CO_2, and ozone. In the infrared, the model uses 25 *k* profiles: 11 for H_2O, 10 for CO_2, and 4 for ozone. This approach allows for the spectral overlap between absorbing species and compares well with line-by-line calculations in the troposphere [*Hansen et al.*, 1983; *Lacis and Oinas*, 1991].

[11] Applying climatological ozone fields derived from observations [*Logan*, 1999a, 1999b] in the radiation scheme, we performed a 125-year control simulation. Climate equilibrium, defined by statistically unvarying globally averaged net radiation at the top of the atmosphere, was achieved by the 25th model year. Doubling CO_2 in the model relative to the present-day yields a climate sensitivity of $0.8°\ C\ m^2\ W^{-1}$, within the range of sensitivity reported for current GCMs [*Ramaswamy*, 2001; *Hansen et al.*, 1997].

[12] Using the Harvard-GISS model in which ozone-NO_x-hydrocarbon photochemistry is embedded within the GCM [*Mickley et al.*, 1999, 2001], we next calculated present-day and preindustrial tropospheric ozone fields. The Harvard-GISS model carries 24 tracers, including five nonmethane hydrocarbons (ethane, propane, >C3 alkanes, >C2 alkenes, isoprene) and their oxidation products. The chemical mechanism includes 80 species (*Horowitz et al.* [1998], with minor updates) and is integrated over a 4-hour timestep. Wet deposition of HNO_3 and H_2O_2 is integrated within the GCM hydrological simulation as described by *Koch et al.* [1999], and dry deposition is carried out using a resistance-in-series scheme [*Wang et al.*, 1998]. Natural and anthropogenic emissions are largely based on *Wang et al.* [1998]. Chemistry in the Harvard-GISS model is implemented in the bottom seven layers of the model, up to about 130 hPa. Monthly mean fluxes of ozone and NO_y across the model tropopause (i.e., between layers 7 and 8) are specified as in the work of *Wang et al.* [1998]. In the tropics, layer 8 lies partly in the troposphere. We refer below to layer 8 as "UT/LS" (upper troposphere/lower stratosphere), but we emphasize that chemistry is performed only up through layer 7. In a comparison with long-term observations, *Mickley et al.* [1999] found that the model captures the present-day monthly mean ozone within about 10 ppb and the seasonal variation within about 1 month.

[13] For the present-day chemistry calculation, methane was set throughout the troposphere at 1.7 ppm. For our "standard" preindustrial calculation, methane was set to 0.7 ppm, all anthropogenic emissions were turned off, biomass burning emissions were scaled to 10% of their present-day value, and natural emissions and the stratospheric ozone and NO_y fluxes were the same as in our present-day simulation [*Mickley et al.*, 1999]. The two simulations were performed for 18 months, and the tropospheric ozone fields for the last 12 months were saved for the climate simulations.

[14] To compute radiative forcing from tropospheric ozone, we apply on-line the GCM radiative transfer code to the calculated present-day and preindustrial ozone fields during the last 12 months of the above simulations, without allowing the ozone forcing to alter climate. We then compare the net longwave and shortwave fluxes at the tropopause for the two simulations and derive the instantaneous radiative forcing. (The tropopause here is again defined as the boundary between layers 7 and 8.) For anthropogenic ozone, we calculate a global and annual mean radiative forcing of $0.49\ Wm^{-2}$, on the high side, but within the range of forcings by other models, $0.3–0.5\ W\ m^{-2}$ [*Ramaswamy*, 2001]. One reason for the higher forcing is that we calculate a greater increase in ozone burden since preindustrial times, 12 DU on average compared to about 7–10 DU reported by other models [*Prather and Ehhalt*, 2001]. Also, we report here the instantaneous forcing, which is 10–20% greater than the adjusted forcing in this model [*Hansen et al.*, 1997]. Our use of instantaneous forcing rather than adjusted forcing, in which the stratospheric temperatures are permitted to adjust to the radiative perturbation, represents a source of uncertainty in this study.

[15] Initializing the model with the meteorological fields from the 25th year of the control simulation, we then performed two 100-year climate equilibrium simulations. In one, the present-day, monthly mean tropospheric ozone fields (layers 1 through 7) were implemented in the radiation scheme; in the other, the preindustrial ozone fields were used. Concentrations of the well-mixed greenhouse gases were held at present-day values for both simulations, and the same climatological ozone distributions were used for the stratosphere (layers 8 and 9). We term the comparison of these two simulations "ΔO_3."

[16] To test the climate sensitivity to the inhomogeneity of tropospheric ozone, we performed a third simulation using tropospheric ozone fields generated by applying a uniform 18-ppb ozone increase to the preindustrial ozone at all levels throughout the troposphere. The 18-ppb increase represents the global and annual mean ozone change calculated by the model since preindustrial times. The strato-

spheric ozone burden is the same as in the ΔO_3 case. For this uniform change in tropospheric ozone, we calculate a global and annual mean radiative forcing of 0.46 W m^{-2}. The label "ΔO_3unif" refers to the comparison between the preindustrial simulation and the simulation with the uniform increase of ozone.

[17] Finally, to identify the climate response unique to an ozone forcing, we repeated the control simulation with a 25 ppm decrease in CO_2. Again we initialized the model with the meteorology generated by the 25th year of the control run. As in the control simulation, climatological ozone was used. The change of 25 ppm CO_2 corresponds to a radiative forcing nearly equivalent to the forcing due to the change in tropospheric ozone from the preindustrial era to the present-day, 0.46 Wm^{-2}. The term "ΔCO_2" refers to the comparison between the control simulation and the simulation with decreased CO_2.

[18] In all four simulations (present-day ozone, preindustrial ozone, preindustrial ozone with uniform ozone change, and control simulation with decreased CO_2), climate equilibrium was reached after about 25 years. We show results averaged over the last 75 years of each of the four simulations. All results unless otherwise specified are significant at the 95% level, as determined by the student's two sample t-test.

[19] A shortcoming of our approach is the reliance on equivalent instantaneous forcings of tropospheric ozone and CO_2 at the tropopause. Adjusted forcings, in which the stratospheric temperatures are permitted to adjust to the perturbed radiative flux, are typically 10–20% less than instantaneous forcings, with a slightly larger decrease for ozone [*Hansen et al.*, 1997]. For ozone, the magnitude of the difference between the adjusted and instantaneous forcing depends in part on the distribution of the ozone changes and on the background ozone concentrations. Using a radiative transfer model and input fields of tropospheric ozone generated by an array of models for the present-day and for the year 2100, *Gauss et al.* [2003] calculated that the adjusted longwave forcing by ozone fields from the Harvard-GISS model was 16% less than the instantaneous longwave forcing. This value is close to the 12% difference calculated by *Hansen et al.* [1997] for a 2 × CO_2 change in a similar GISS model. In our view, comparing the climate response to changes in ozone and CO_2 with equivalent adjusted forcings, rather than equivalent instantaneous forcings as we have done here, would have made little difference to our main conclusions.

3. Results

[20] Figure 1 shows the zonally and annually averaged change in tropospheric ozone since preindustrial times calculated by the Harvard-GISS model. The greatest ozone increases, 25–30 ppb, appear in the upper and lower troposphere over northern middle to high latitudes. Figure 2 shows the calculated change in tropospheric column ozone since preindustrial times for December–January–February (DJF) and June–July–August (JJA), and the corresponding radiative forcing as a sum of longwave and shortwave forcing. The plots of ozone column change show the influence of biomass burning in sub-Saharan Africa in DJF and the large increases in Northern Hemisphere summer due to the combination of industrial emissions and summer insolation. At high northern latitudes in Northern Hemisphere summer, upper tropospheric ozone increases significantly due to transport of ozone precursors to that region, long hours of sunlight, and the long chemical lifetime of ozone at high altitudes. The calculated forcings are as great as 1.2 Wm^{-2} over the Arctic in summer, when shortwave forcing over ice becomes especially important due to absorption of both incident and reflected sunlight.

[21] Figure 3 shows the annually averaged radiative forcings for the 25-ppm increase in CO_2 and for the 18-ppb uniform change in ozone. (For the CO_2 pair of simulations, we report the results as the control value minus the value in the simulation with decreased CO_2. Thus we describe here the effect of an increase in CO_2.) For both calculations, the patterns of radiative forcing are generally symmetric about the equator, with the strongest forcing over low latitudes, where the temperature contrast between the earth's surface and the tropopause is greatest [*Mickley et al.*, 1999]. The bottom left panel, which shows the difference between the ΔO_3unif and ΔCO_2 forcings, reveals that the uniform ozone change results in a steeper latitudinal gradient in forcing than the CO_2 change. A clue to this difference lies in the bottom right panel, which shows the difference in forcing for ΔO_3unif and ΔCO_2 when the interference due to water vapor is removed from the forcing calculations by assuming a water-free atmosphere in that part of the model code. Water vapor absorbs strongly in the infrared and its presence can swamp the forcing from other gases, particularly over the moist tropics. The absorption cross sections of water vapor overlap to a greater extent with those of CO_2 than with those of ozone [*Lenoble*, 1993], so removing water vapor leads to relatively greater forcing over the tropics for ΔCO_2 than for ΔO_3unif, and the difference between the two forcings in that region is halved.

[22] Figure 4 shows the annual global mean vertical profiles of the shortwave, longwave, and total forcing for the three cases. Shortwave forcing by ozone is negative at the surface and increases gradually with altitude, becoming positive in the midtroposphere; the added ozone allows less sunlight to penetrate to the lowest layers of the atmosphere, leading to net cooling in the shortwave. In the middle to upper troposphere, the added ozone absorbs not just incident sunlight but also reflected sunlight that would otherwise escape to space, leading to net shortwave warming. For ΔCO_2, the shortwave forcing is small and slightly negative since CO_2 added to the stratosphere diminishes the downward solar flux to the troposphere by a small amount.

[23] In the longwave, the ozone and CO_2 forcings are positive throughout. For all three cases, the longwave forcing in the lowest layers of the troposphere is sharply reduced due to the presence of water vapor and clouds. Again because the overlap between CO_2 and water vapor cross sections is much greater than for ozone and water vapor [*Lenoble*, 1993], the longwave forcing for CO_2 increases rapidly with altitude as water vapor concentrations fall off. Above about 4 km, however, the CO_2 forcing is relatively constant with height as a result of saturation in the CO_2 absorption bands. In contrast, tropospheric ozone is optically thin, and therefore the corresponding radiative

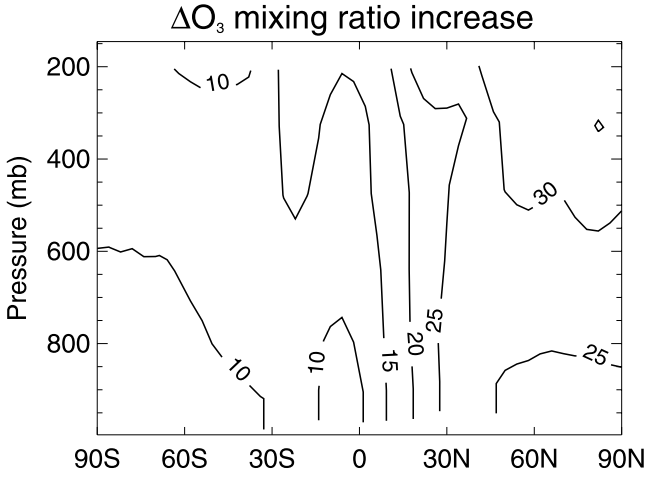

Figure 1. Zonally averaged, annual mean change in tropospheric ozone from preindustrial times to the present day, as calculated by the Harvard-GISS model. Units are ppb.

forcing increases more gradually with altitude through the depth of the tropospheric column. Multiplying the ozone concentrations by 1000 in a sensitivity calculation (to make it optically thick) results in a longwave forcing profile for ozone similar in shape to that of CO_2 forcing (not shown). In the upper troposphere, the ozone longwave forcing increases with height due to colder temperatures aloft. We see that for the same radiative forcing at the tropopause, an increase in CO_2 deposits about twice as much heat in the middle troposphere as an increase in tropospheric ozone. This results in significantly greater surface warming from the increase in CO_2, as presented below.

[24] We next examine the results of the climate simulations. Figure 5 shows the profile of the globally averaged, annual mean temperature differences for the three cases ΔO_3, ΔO_3unif, and ΔCO_2. Results for ΔO_3 show a surface warming of 0.28°C, a slightly greater warming in the upper troposphere, and a strong cooling, about 0.2°C, in the UT/LS. We examine this cooling in greater detail below and show that most of it occurs over high latitudes in the lower stratosphere. Results for ΔO_3unif are almost identical. Figure 6 presents vertical profiles of the hemispheric

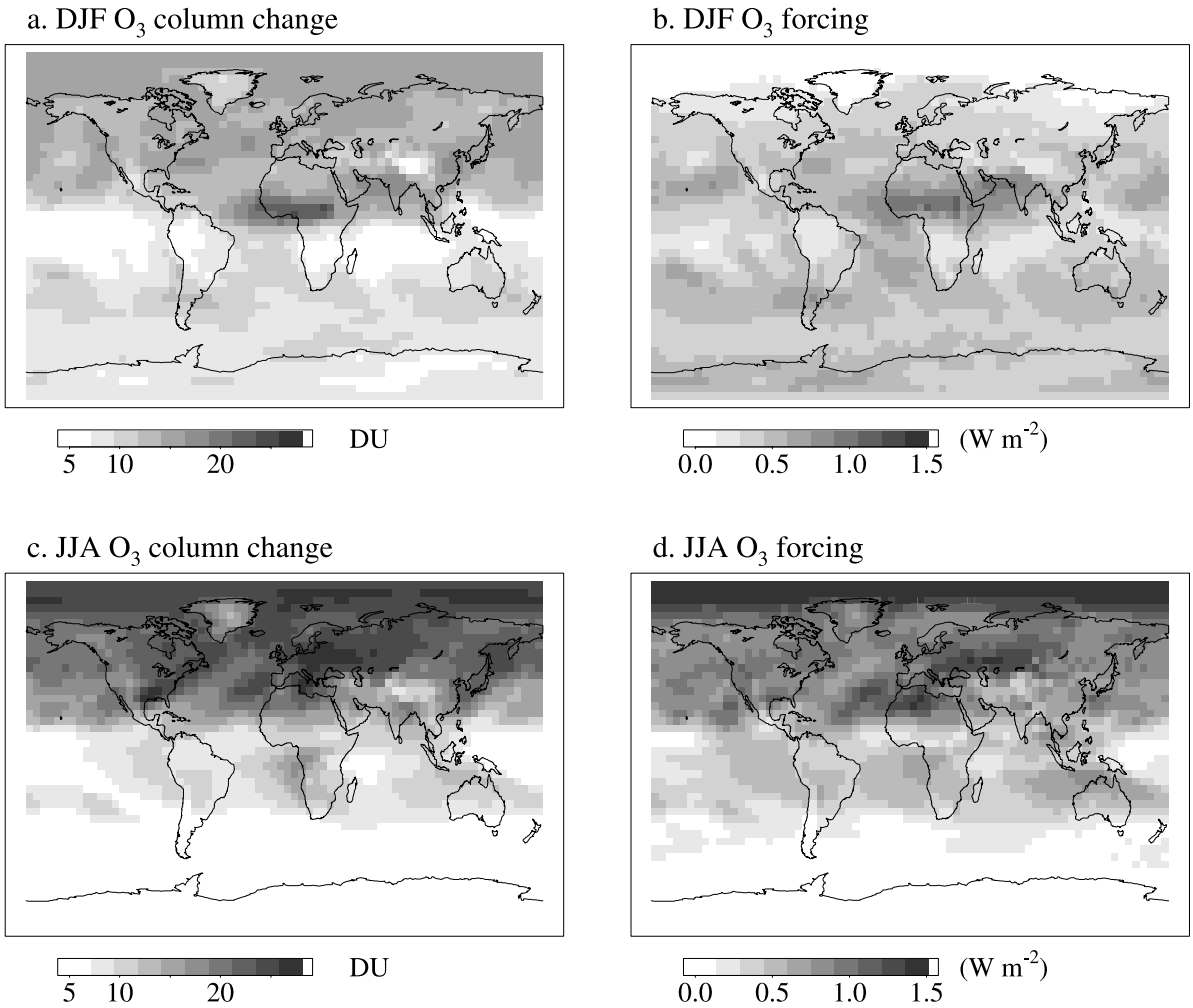

Figure 2. Calculated column change of tropospheric ozone since preindustrial times in Dobson units (DU) and the corresponding instantaneous radiative forcings at the tropopause in W m^{-2} for DJF (a, b) and JJA (c, d). See color version of this figure at back of this issue.

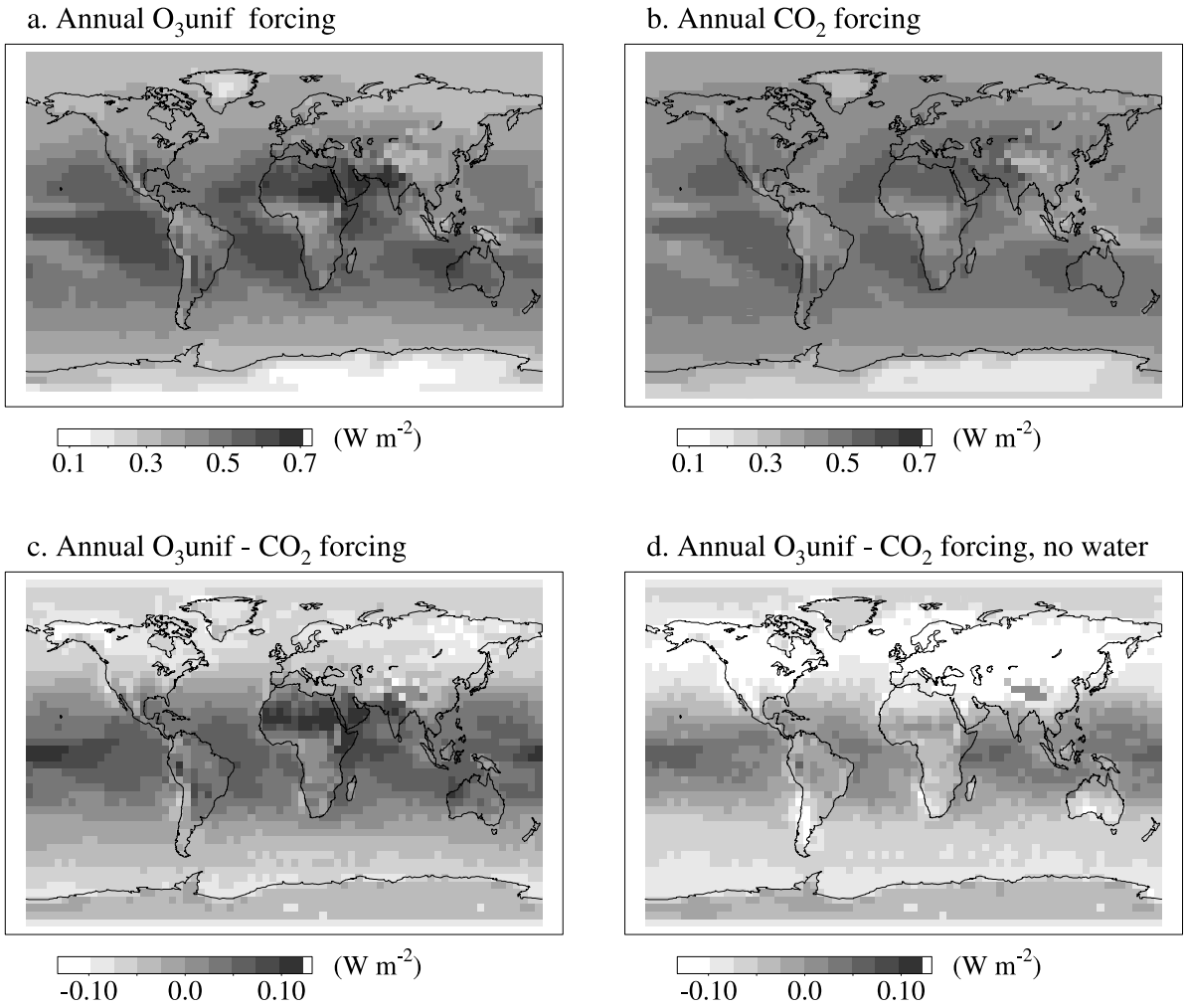

Figure 3. Calculated, annual mean, instantaneous forcing at the tropopause due to (a) an 18-ppb increase in tropospheric ozone applied uniformly throughout the troposphere to preindustrial ozone and (b) a 25-ppm increase in CO_2. Figure 3c shows the difference between these two forcings; Figure 3d shows the difference when the interference due to water vapor is excluded from the calculation. See color version of this figure at back of this issue.

mean temperature changes due to increasing ozone. For ΔO_3, the temperature increase at the surface is nearly 0.2°C greater in the Northern than in the Southern Hemisphere. For ΔO_3unif, the surface temperature difference between the two hemispheres is only 0.03°C, indicating the effect of the inhomogeneity of the ΔO_3 forcing (Figures 1 and 2).

[25] We see from Figure 5 that the surface warming for ΔCO_2 (0.36°C) is about 30% greater than the surface temperature response to increases in ozone, either calculated or uniformly applied. As in the ΔO_3 and ΔO_3unif cases, the temperature change for ΔCO_2 maximizes in the upper midtroposphere. In the UT/LS, however, the increased CO_2 leads to a slight increase in temperature, 0.05°C, in contrast to the cooling exhibited by the ΔO_3 and ΔO_3unif cases. Most of that warming occurs over the tropics. Farther up in the stratosphere (at the highest model level), where increases in greenhouse gases increase the upwelling longwave radiation flux [*Andrews et al.*, 1987], ΔCO_2 shows strong cooling, about 0.3°C.

[26] A standard normalized measure of climate response to a radiative perturbation is the climate sensitivity parameter, defined as the change in global mean surface temperature per unit change in global radiative forcing [*Houghton et al.*, 1993]. We calculate a climate sensitivity parameter for tropospheric ozone of 0.6°C m^2 W^{-1}, significantly less than for CO_2 (0.8°C m^2 W^{-1}). To remove the altitude sensitivity of the temperature response, we have also calculated the annual mean, pressure-weighted temperature changes for the three cases, integrated over the model troposphere (layers 1–7). Again we find a stronger sensitivity to ΔCO_2 than for the ozone cases, with mean tropospheric temperature increases of 0.38°C for the ΔCO_2 case and 0.29°C for both the ΔO_3 and ΔO_3unif cases. The stronger sensitivity to ΔCO_2 is consistent with the results of *Joshi et al.* [2003], who applied a uniform increase to upper tropospheric ozone. In the Discussion section, we explore the reasons for the greater sensitivity of climate to ΔCO_2 relative to the two ozone cases and compare our results to previous studies.

[27] We next examine in greater detail the geographic inhomogeneity and seasonal variation of the climate re-

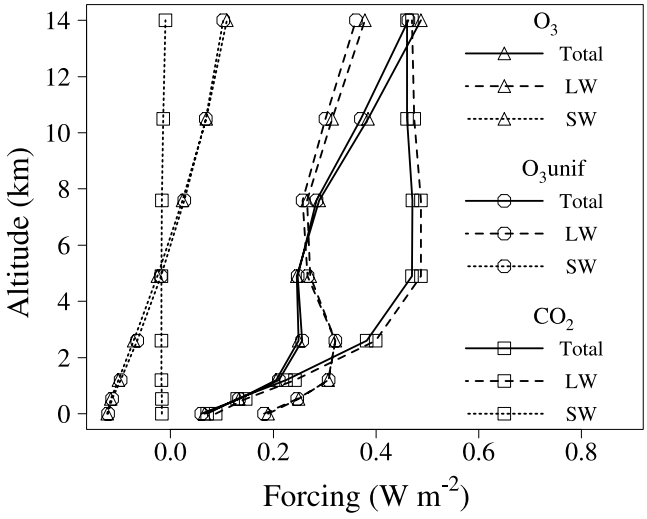

Figure 4. Vertical distribution of radiative forcing for (a) the calculated ozone increase from preindustrial times to the present-day (blue curves, triangles), (b) an equivalent 18-ppb increase of ozone (green curves, circles), and (c) a 25-ppm CO_2 increase (red curves, squares). The dashed curves denote the longwave forcings; the dotted curves, the shortwave forcings; and the solid curves, the total (longwave + shortwave) forcings. Values are annual global means. The forcings represent values at the edges of the model layers, beginning at the bottom with the forcing at the Earth's surface. See color version of this figure at back of this issue.

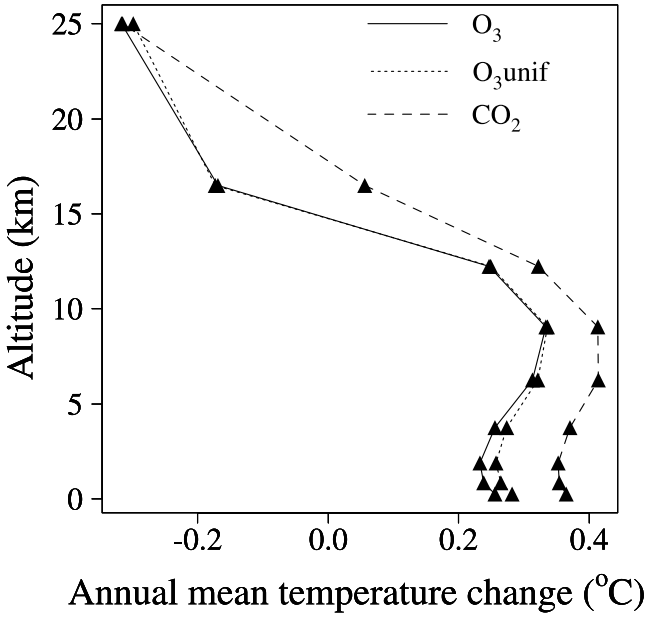

Figure 5. Annual and global mean temperature response as a function of altitude for (a) our calculated increase of tropospheric ozone since preindustrial times (solid curve), (b) an equivalent 18-ppb uniform increase of ozone (dotted curve), and (c) a 25-ppm increase of CO_2 (dashed curve).

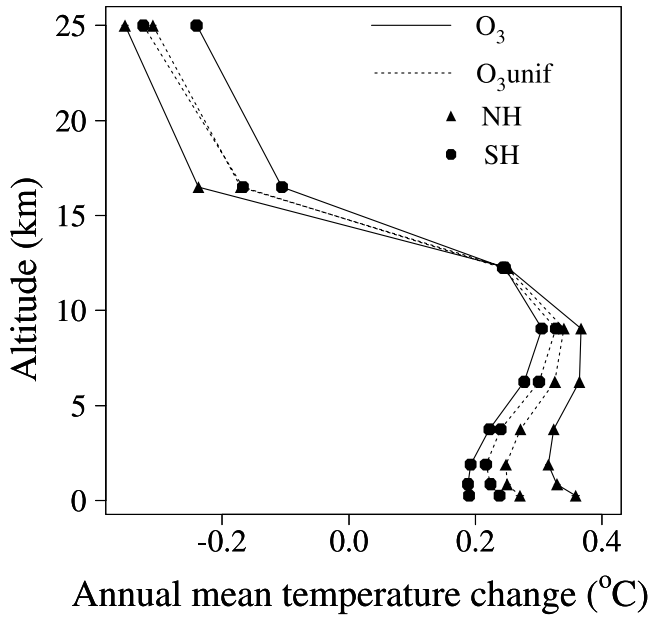

Figure 6. Annual mean temperature response as a function of altitude for our calculated increase of ozone since preindustrial times (solid curves) and an equivalent 18-ppb uniform increase of ozone (dotted curves). The triangles represent the Northern Hemisphere averages, and the circles are for the Southern Hemisphere.

sponse to changes in ozone and CO_2. We also investigate the changes in clouds and other meteorological variables that result from the greenhouse gas perturbations.

[28] Figure 7 presents the zonally averaged DJF (top panel) and JJA (bottom panel) surface temperature response for the three cases. At high northern latitudes, a positive feedback loop operates in which surface warming reduces snow and ice coverage and thus albedo, leading to still greater temperatures. The diminished sea ice also exposes warm surface waters to the cold winter air, transferring more heat to the atmosphere. The albedo feedback effect is especially apparent in DJF for the ΔCO_2 case, since the CO_2 forcing, unlike the forcing for ozone, does not depend on incoming solar radiation and is double the ΔO_3 forcing at high latitudes in winter. Further amplifying the sensitivity of DJF surface temperature in the ΔCO_2 case at high latitudes is a 1% increase in low cloud cover (not shown). In the Southern Hemisphere, the positive feedback is muted in JJA and absent in DJF for all three cases since the albedo of ocean ice in the Southern Hemisphere has been specified at a low value, providing little contrast with the albedo of open water.

[29] Figure 8 shows the seasonal variation of the global mean surface and tropospheric temperature responses for the three cases. While the ΔCO_2 case exhibits the strongest surface temperature response during Northern Hemisphere winter, driven by the positive ice albedo effect noted above, the ΔO_3 and ΔO_3unif cases show little seasonal change. For the ΔO_3 case, however, the mean tropospheric temperature response exhibits a steep increase in Northern Hemisphere summer due to large ozone increases at that time of year and strong heating in the middle and lower troposphere. The zonally averaged surface temperatures, however, do not

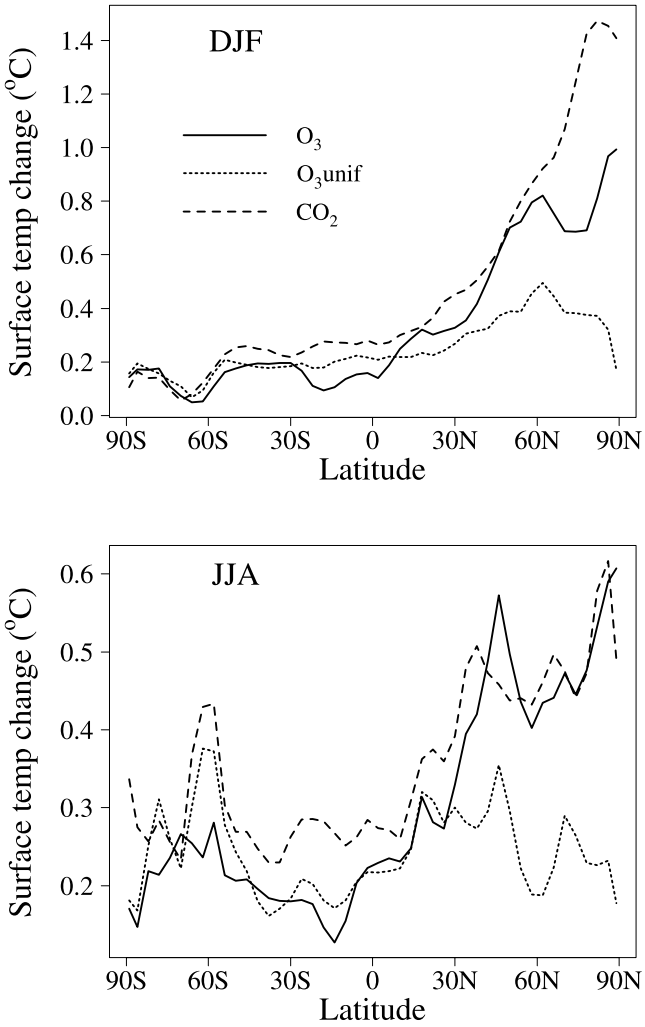

Figure 7. Zonally averaged increases in surface air temperatures in DJF (top) and JJA (bottom) for (a) our calculated increase in tropospheric ozone since preindustrial times (solid curves), (b) an equivalent 18-ppb uniform increase in ozone (dotted curves), and (c) a 25-ppm increase in CO_2 (dashed curves).

reflect this strong summertime heating since convection distributes the heat through the column.

[30] In Figure 9 we compare vertical profiles of the globally averaged changes in cloudiness for the three cases. All three cases exhibit reduced cloud cover at low altitudes and increased cloud cover at high altitudes. Both these changes amplify the surface temperature response to a greenhouse gas warming [*Hansen et al.*, 1997]. The ΔCO_2 case exhibits especially large responses in cloud cover at these two heights, nearly double the response of the ΔO_3 case, which contributes to the greater climate sensitivity to the CO_2 increase. We will return to this point in the Discussion section.

[31] In Figure 10 we show the horizontal distribution of the mean JJA surface temperature response for the three cases as well as the difference between the ΔO_3 and ΔCO_2 cases. White areas indicate regions of insignificant differences as determined by the student's two sample t-test. At this time of year, ΔO_3 yields strong surface warming, 0.8–1°C, downwind of source regions (Europe and Asia) and over the continental interior of North America and Australia. The relatively large effects over continental regions are due to preferential heating of the boundary layer, where anthropogenic ozone is abundant, resulting in reduced low cloud cover and amplification of the warming. For example, over the southern United States, coincident with the largest increases in column ozone in the lower troposphere, surface temperature increases by about 1°C, static stability in the lower troposphere decreases by 0.1°C km^{-1}, low cloud cover decreases by 2%, and precipitation decreases by 0.3 mm d^{-1}. Over the same region, the ΔO_3unif and ΔCO_2 cases do not show significant meteorological changes other than temperature increases. The ΔCO_2 case, however, exhibits strong temperature increases over the dry Saharan region, where little water vapor interferes with CO_2 absorption and a decrease in cloud cover (~2%) amplifies the response.

[32] We caution against overinterpretation of the downwind temperature response to increased tropospheric

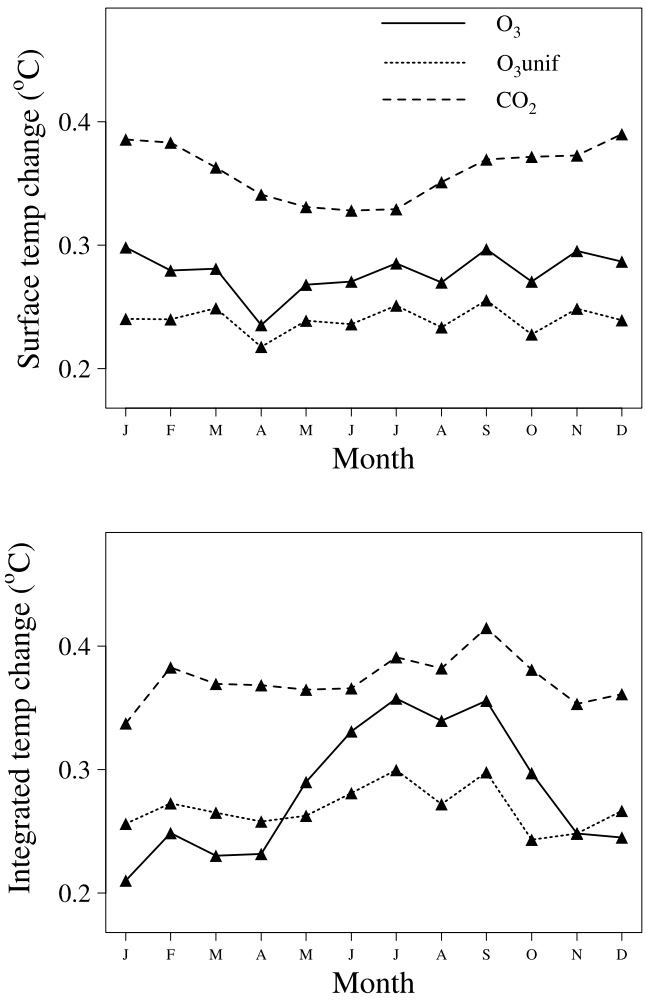

Figure 8. Seasonal changes in global mean surface temperature (top) and mean tropospheric temperature (bottom) due to (a) our calculated increase in tropospheric ozone since preindustrial times (solid curves), (b) an equivalent 18-ppb uniform change in ozone (dotted curves), and (c) a 25-ppm increase in CO_2 (dashed curves).

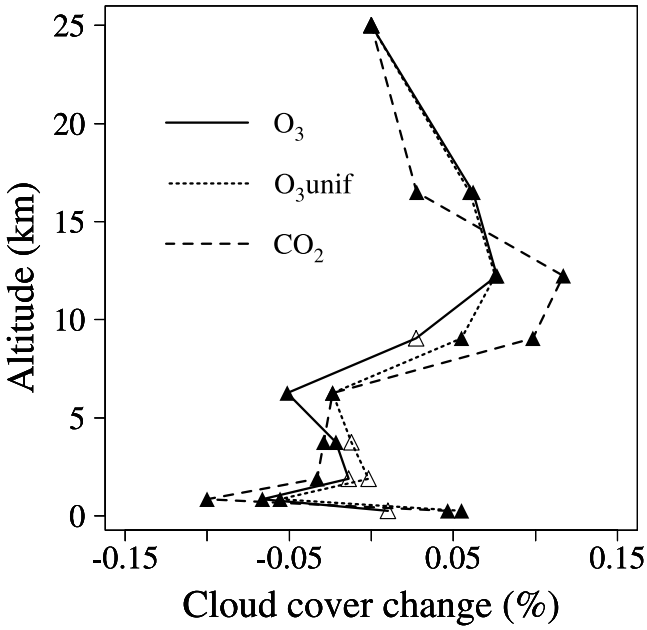

Figure 9. Annual mean response of cloud cover as a function of altitude for the calculated increase of tropospheric ozone since preindustrial times (solid curve), an equivalent 18-ppb increase in tropospheric ozone (dotted curve), and a 25-ppm increase in CO_2 (dashed curves). The filled triangles represent changes significant at the 95% level as determined by the student's two-sample t-test; the empty triangles denote insignificant changes.

ozone. Heterogeneous forcings do not always map onto climate response; local feedbacks play a major role in determining climate sensitivity [*Boer and Yu*, 2003]. However, as is clear in Figure 10, the surface temperature response to ΔO_3 differs substantially from the response to ΔCO_2, and these differences can be explained only by the geographical pattern or wavelength dependence of the ozone forcing. Interestingly, *Boer and Yu* [2003] calculate a strong cooling downwind of Asia in response to aerosol forcing, similar to the warming we calculate here for ΔO_3.

[33] Figure 11 shows the longitudinal variation in selected ΔO_3 climate variables across the equatorial Pacific (2–6 S), from 100 E (Indonesia) to 80 W (South America) in JJA. For ease of comparison, all changes have been normalized by the maximum of the absolute values for each change, and only the significant changes are shown. Outflow of biomass burning pollution from Asia and South America, carried by the Walker circulation, leads to the greatest ozone column changes on either side of the Pacific, with a minimum in column change at the warm pool east of Indonesia, a region of intense convection. The radiative forcing correlates with the column change, supplying heat to upper altitudes and stabilizing the troposphere. Over Indonesia vertical motion decreases in response to the ozone change (-2×10^{-4} m s^{-1}), as well as high cloud cover (−3%), and precipitation (−1 mm d^{-1}). Stronger easterlies (+0.5 m s^{-1}) appear on either side of the warm pool, drawing moist air to that region and generating a large increase in surface temperature (+0.3°C). By contrast, the ΔCO_2 and ΔO_3unif cases exhibit little longitudinal variation in forcing or climate response across the Pacific.

[34] In Figure 12, we show the zonally averaged DJF temperature response for ΔO_3, ΔCO_2, and ΔO_3unif in the UT/LS model layer (about 16 km or 100 hPa). The plot indicates that the temperature decrease for ΔO_3 and ΔO_3unif is greatest over the dark, wintertime Arctic with values as large as −1°C. At these latitudes, the UT/LS layer lies entirely in the stratosphere. Our result suggests that at low levels of solar insolation, the stratospheric heat budget is especially sensitive to changes in the upwelling terrestrial flux at the ozone absorption wavelengths, 9.6 and 14 μm. We note that in models with more sophisticated representations of the stratosphere, the climate response to changing greenhouse gases over the Arctic is harder to detect due to interannual, dynamic variability [e.g., *Ramaswamy and Schwarzkopf*, 2002]. Over the tropics, where this layer lies partly in the troposphere, the ΔCO_2 case shows a slight warming (0.05°C).

4. Discussion

[35] This study attempts to identify the unique response of climate to realistic changes in the abundance of tropospheric ozone. We have conducted climate equilibrium calculations in a general circulation model with present-day and preindustrial tropospheric ozone concentrations and compared the resulting ΔO_3 climate response to the response generated by a uniform, 18-ppb increase of tropospheric ozone (ΔO_3unif) and by a 25-ppm increase in CO_2 (ΔCO_2) all of which yield the same global instantaneous radiative forcing (0.46–0.49 W m^{-2}).

[36] We find that a 0.49 W m^{-2} radiative forcing due to anthropogenic tropospheric ozone corresponds to a global mean surface temperature change of 0.28°C, with significantly greater surface warming in the Northern Hemisphere than in the Southern Hemisphere (0.39°C versus 0.17°C), because of the greater abundance of anthropogenic ozone in the north. The ΔO_3unif case yields nearly identical surface temperature increases in both hemispheres of about 0.26°C. For both cases, a model with a more realistic sea ice albedo in the Southern Hemisphere would likely exhibit a greater climate response in that hemisphere. The preindustrial ozone fields in our simulations were calculated with a standard tropospheric chemistry model, which, like most other models, overestimates preindustrial ozone compared to observations from the late 19th century. We have shown in previous work that varying the natural emissions of ozone precursors in the model within their uncertainties could provide a better match to the 19th century observations and yield a radiative forcing from tropospheric ozone of up to 0.80 W m^{-2} [*Mickley et al.*, 2001; *Shindell and Faluvegi*, 2002]. The corresponding temperature increases would likely be about 60% higher than those reported here.

[37] For the ΔCO_2 case, the globally averaged surface temperature increases by 0.36° C, indicating a 30% greater sensitivity of surface temperature to increases in CO_2 than to ozone for the same global radiative forcing. Our results are consistent with *Stuber et al.* [2001] and *Joshi et al.* [2003], who reported CO_2 climate sensitivities 20–60% greater than the sensitivities to uniform increases of upper tropospheric ozone. *Christiansen* [1999], using a GCM with

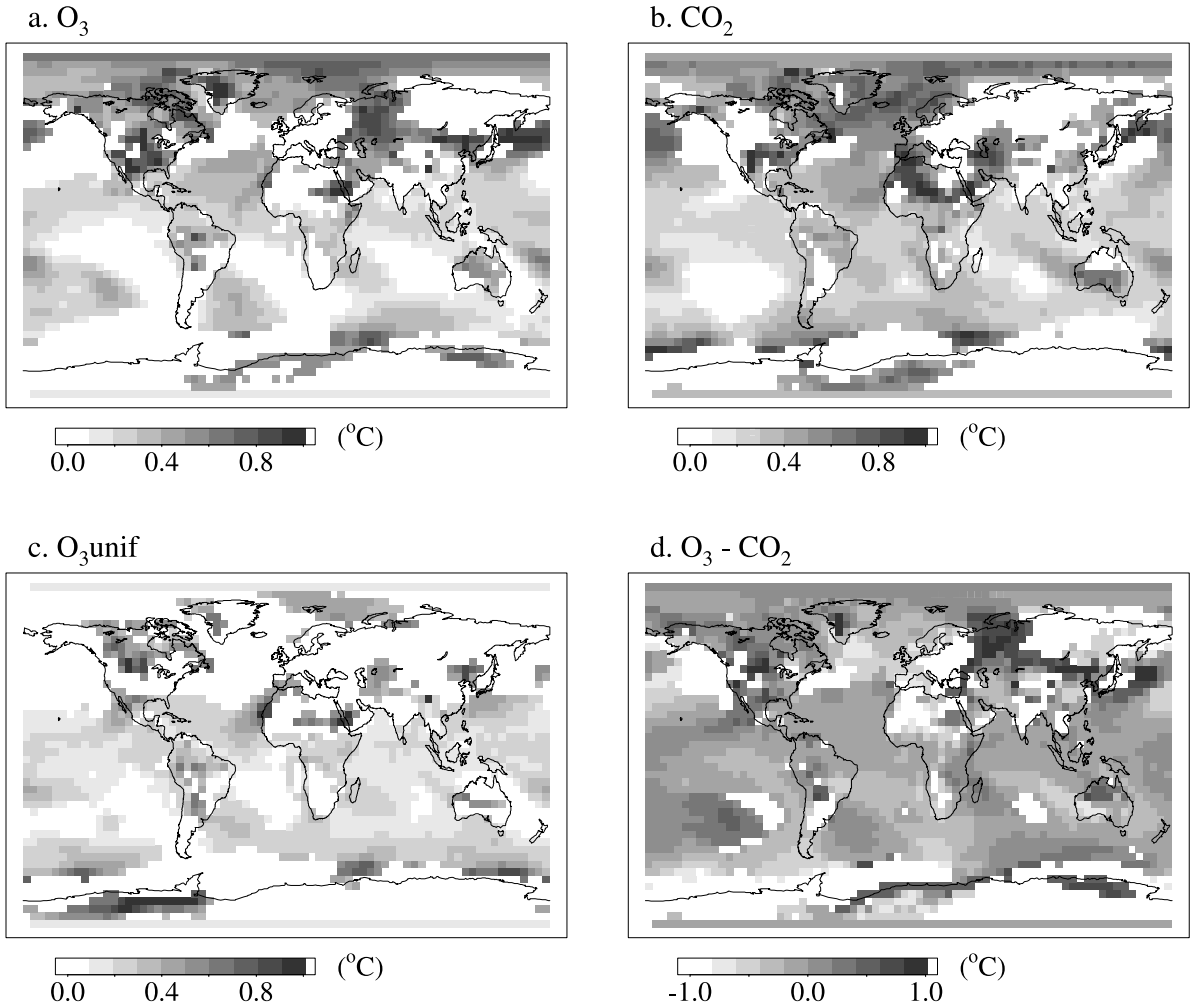

Figure 10. JJA surface temperature response to (a) the calculated increase in ozone, (b) the 25-ppm increase in CO_2, and (c) the 18-ppb uniform change in ozone. Figure 10d shows the difference in surface temperature response between the calculated ozone case and the CO_2 case. White areas indicate insignificant values at the 95% level as determined by the student's two sample t-test. In calculating differences in Figure 10d, insignificant values were assumed to be zero. See color version of this figure at back of this issue.

perpetual January conditions, reported nearly similar climate sensitivities for changes in CO_2 and ozone but kept sea ice coverage constant and increased ozone uniformly throughout the troposphere.

[38] Given the complexity of the model meteorology, it is difficult to pin down all the causes for the difference in sensitivity between ΔCO_2 and the two ozone cases. One likely reason is that the poleward shift in radiative forcing of ΔCO_2 compared with ΔO_3 (Figure 3) leads to a stronger ice albedo feedback and thus to stronger warming. While the forcings for ΔO_3 over the Arctic are as great or greater than those of ΔCO_2, it is probably of consequence that the ΔO_3 forcings in this region operate mainly during the Northern Hemisphere summer, while the ΔCO_2 forcings affect the Arctic year-round. For ΔCO_2, the increase of low cloud cover during Arctic winter further amplifies the surface temperature response. Globally, the increased ozone in the upper troposphere may increase the static stability in that region and reduce the coupling between the surface and the tropopause [*Joshi et al.*, 2003]. In our model, the globally averaged increase in static stability for the troposphere as a whole was very small and similar in all cases ($\sim$0.005°C km^{-1}). For ΔO_3 in JJA only, the zonally averaged static stability in the upper troposphere (between 500 and 130 hPa) increased over low latitudes, 0.14°C km^{-1} versus 0.05°C km^{-1} for ΔCO_2, consistent with *Joshi et al.* [2003].

[39] Finally, and perhaps most importantly, an identical radiative forcing for ozone and CO_2 at the tropopause implies in fact a greater amount of heating by CO_2 in the middle troposphere because CO_2 is optically thick whereas ozone is optically thin (Figure 4 and related discussion). *Hansen et al.* [1997], applying "ghost forcings" of 4 Wm^{-2} at various levels in the troposphere in the GISS GCM and allowing cloud feedbacks to operate, calculated a 30–40% stronger temperature response to forcings applied to the middle troposphere than to the upper troposphere. The midtroposphere forcings increased high cloud cover and thus amplified the surface temperature response, while the

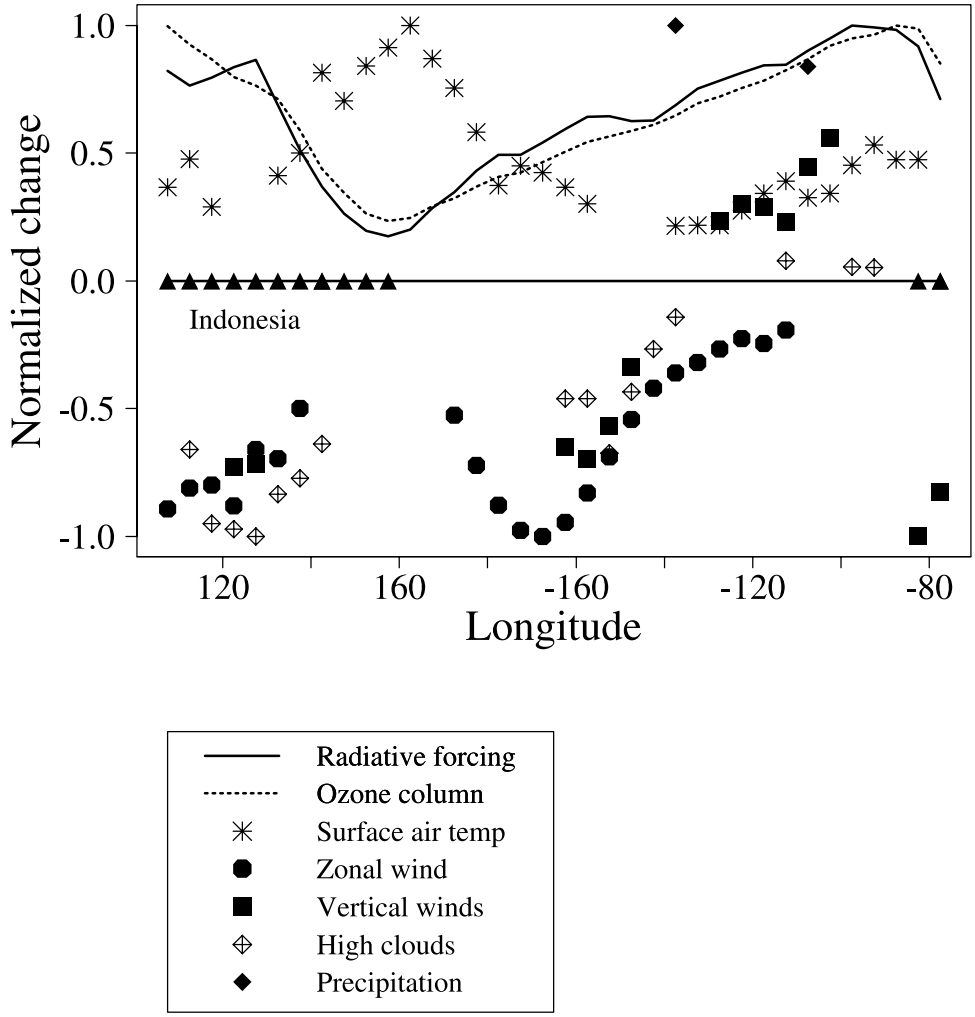

Figure 11. Normalized meteorological changes due to the calculated ozone increase over the equatorial Pacific since preindustrial times (mainly biomass burning), as a function of longitude. Variables are averaged over the 2–6 S latitude band and normalized to the maximum absolute values of each change. The solid gold curve denotes the ozone column change between the surface and the tropopause and the dotted brown curve shows the corresponding radiative forcing. The symbols show the changes in surface air temperature, surface zonal wind, vertical winds, high cloud cover, and precipitation. Only significant changes are shown. The black triangles denote longitude bands that contain land. See color version of this figure at back of this issue.

upper troposphere forcings reduced high cloud cover via local heating. We thus argue that the surface temperature responds not just to the tropopause forcing but also to the vertical profile of radiative imbalances through the troposphere. *Christiansen* [1999], in his estimation of the climate response to a uniform change of stratospheric ozone compared to that of a uniform change in tropospheric ozone, points out that the vertical partitioning of radiative forcing plays a major role in determining climate sensitivity to a perturbation. In that study, the stratospheric ozone forcing, deposited mainly at the Earth's surface, led to a greater surface temperature response than the tropospheric ozone forcing, deposited mainly in the free troposphere. Here we show that the CO_2 forcing, deposited through the troposphere, generates a stronger climate response than a realistic ozone forcing, which is largest in the upper troposphere.

[40] In a previous study, *Boer and Yu* [2003] have shown that to first order two very different radiative perturbations (sulfate aerosol and well-mixed greenhouse gases) generate a similar pattern in surface temperature response. To some degree our work supports this conclusion: we see stronger warmings in the Northern Hemisphere, particularly at high latitudes where the positive ice-albedo feedback operates. However, our work also highlights the particularities of the climate response to changing tropospheric ozone. For example, we show that anthropogenic ozone leads to strong surface warming over continental interiors, intensified by significant decreases in static stability and low cloud cover. Our work suggests that the low cloud cover response to increased ozone may accelerate photolysis rates and enhance ozone production in a positive feedback loop. The decrease in static stability may lift anthropogenic ozone to higher altitudes, further amplifying its radiative forcing.

[41] We find in the model that increasing tropospheric ozone since preindustrial times has led to cooling of the

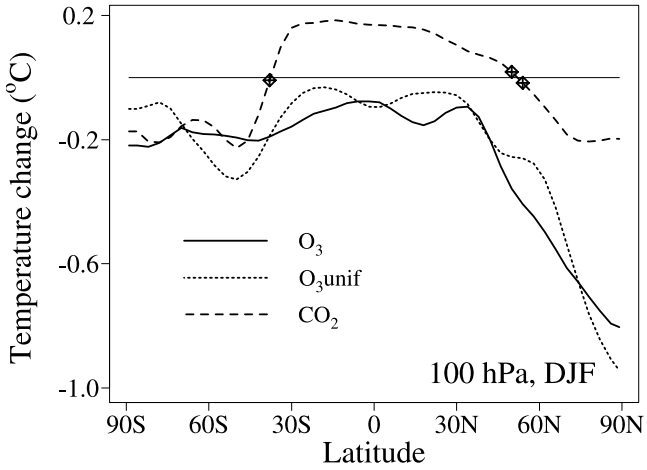

Figure 12. Zonally averaged DJF temperature response in the UT/LS layer (upper troposphere/lower stratosphere, about 100 hPa) for (a) our calculated increase in tropospheric ozone since preindustrial times (solid curves), (b) an equivalent 18-ppb uniform increase in ozone (dotted curves), and (c) a 25-ppm increase in CO_2 (dashed curves). The diamonds indicate gridpoints with insignificant temperature differences for the ΔCO_2 case. At high latitudes, the UT/LS layer lies entirely in the stratosphere.

lower stratosphere by nearly 1°C over the Arctic in winter. Earlier, *Ramaswamy and Bowen* [1994] had noted a similar effect in a one-dimensional (1-D) radiative-convective model: decreasing lower stratospheric ozone heated the upper stratosphere due to the perturbation in the 9.6 μm radiative transfer. Using the fixed dynamical heating (FDH) approximation in a 3-D radiative model with coarse horizontal resolution (8° × 10°), *Berntsen et al.* [1997] later calculated lower stratosphere cooling, mainly between 15 and 50 N, in response to increased tropospheric ozone. Using a GCM and applying uniform upper tropospheric ozone increases, both *Stuber et al.* [2001] and *Joshi et al.* [2003] found that the lower stratosphere at 60 N cooled about 1°C. Our results confirm these earlier findings for a realistic ozone response within a GCM.

[42] The calculated cooling of the lower stratosphere at high latitudes has implications for the recovery of the stratospheric ozone layer in the coming years as chlorine levels decline. Recent work suggests that increased concentrations of the long-lived greenhouse gases may reduce the frequency of sudden stratospheric warmings, leading to colder temperatures, greater concentrations of polar stratospheric clouds, and more severe wintertime ozone loss within the Arctic vortex [*Shindell et al.*, 1998]. Our work implies that future increases in tropospheric ozone [*Prather et al.*, 2003] may further depress temperatures in the Arctic vortex in winter and add to the delay in ozone recovery in the lower stratosphere in that region. On the other hand, away from polar regions, the stratospheric cooling caused by increasing tropospheric ozone may contribute to a more rapid recovery of stratospheric ozone [*Rosenfield et al.*, 2002].

[43] Our specific finding that anthropogenic ozone reduces vertical motion, high cloud cover, and rainfall over Indonesia has important implications. The rapid economic development in Africa and Asia in the coming years will likely lead to continued convective outflow of high levels of pollution to the Pacific. The subsequent decrease in cloud cover and rainfall over Indonesia due to ozone heating aloft may alter the monsoon meteorology, as less latent heat would be released by condensation. A decline in rainfall over Indonesia may also exacerbate biomass burning events, such as the one that occurred in 1997 during a particularly severe El Nino year. Our calculations probably underestimate the effects of rising ozone levels in this region: in a fully coupled model, increased convection over the warm pool could sharpen the horizontal gradients in ozone column change and strengthen the climate response.

[44] In all our calculations, the climate response to the greenhouse gas forcings is damped by the insensitive ocean ice albedo of the Southern Hemisphere. In addition, our model vertical resolution is too coarse to capture the sharp temperature or ozone gradients at the tropopause and has a limited representation of the stratosphere and boundary layer [*Rind et al.*, 2001]. These model weaknesses could influence the calculation of tropopause forcing and the resulting climate response. For example, finer vertical resolution could allow for more convection [*Rind and Lerner*, 1996], leading to stronger coupling between the tropopause and surface and a stronger temperature response. In an intercomparison of calculated ozone perturbations for 2100 that included results from our model, *Gauss et al.* [2002] found that the coarse resolution of the GISS GCM led to an underestimate of the ozone change and thus the ozone forcing since the tropical tropopause had been set too low in our chemistry calculations. In any event, increasing the vertical resolution would probably not change the vertical profiles of forcing significantly, and the gap between the ozone forcings and the CO_2 forcing in the midtroposphere would no doubt remain. However, increased vertical resolution in the stratosphere would allow us to assess with greater confidence the significance of the radiative cooling in that region that we calculate with increased tropospheric ozone. Also, the use of equivalent instantaneous forcings, rather than equivalent adjusted forcings, is another shortcoming. Finally, the small but realistic forcings employed here mean that some regions experience little significant climate response. Averaged globally or even zonally, however, the signals do attain statistical significance.

[45] Our work demonstrates the limitations in the use of radiative forcing as a measure of the relative importance of greenhouse gases to climate change. Recent work has suggested that cutting back emissions of methane and ozone precursors may be politically more palatable than reducing CO_2 emissions and will lead to a significant decline in the rate of global warming [*Hansen et al.*, 2000]. While on a global scale CO_2 appears to be a more effective "global warmer" than tropospheric ozone per unit forcing, regional sensitivities to increased ozone may lead to strong climate responses on a regional scale. In addition, the dramatic temperature response in the high latitude lower stratosphere in winter to increases in tropospheric ozone suggests that controlling tropospheric ozone abundances will provide the unexpected benefit of hastening recovery of polar stratospheric ozone.

[46] **Acknowledgments.** This work was funded by the NASA Interdisciplinary Science (IDS) Program of the NASA Earth Observatory System (EOS). The authors thank two anonymous reviewers for their detailed suggestions and Reto A. Ruedy, Dylan B. Jones, and Andrew A. Lacis for helpful discussions.

References

Andrews, D. G., J. R. Holton, and C. B. Leovy (1987), *Middle Atmospheric Dynamics*, 489 pp., Academic, San Diego, Calif.

Berntsen, T. K., I. S. A. Isaksen, G. Myhre, J. S. Fuglesvedt, F. Stordal, T. Alsvik Larsen, R. S. Freckleton, and K. P. Shine (1997), Effects of anthropogenic emissions on tropospheric ozone and its radiative forcings, *J. Geophys. Res.*, *102*, 28,101–28,126.

Boer, G. J., and B. Yu (2003), Climate sensitivity and response, *Clim. Dyn.*, *20*, 415–429.

Christiansen, B. (1999), Radiative forcing and climate sensitivity, *Q. J. R. Meteorol. Soc.*, *125*, 3011–3035.

Chung, C. E., V. Ramanathan, and J. T. Kiehl (2002), Effects of the south Asian absorbing haze on the northeast monsoon and surface-air heat exchange, *J. Clim.*, *15*, 2462–2476.

Hansen, J., I. Fung, A. Lacis, D. Rind, S. Lebedeff, R. Ruedy, and G. Russell (1988), Global climate changes as forecast by Goddard Institute for Space Studies three-dimensional model, *J. Geophys. Res.*, *93*, 9341–9364.

Hansen, J., M. Sato, and R. Ruedy (1997), Radiative forcing and climate response, *J. Geophys. Res.*, *106*, 6831–6864.

Hansen, J., M. Sato, R. Ruedy, A. Lacis, and V. Oinas (2000), Global warming in the twenty-first century: An alternative scenario, *Proc. Nat. Acad. Sci. USA*, *97*, 9875–9880.

Hansen, J., and M. Sato (2001), Trends in measured climate forcing agents, *Proc. Nat. Acad. Sci. USA*, *98*, 14,778–14,783.

Hansen, J., et al. (2002), Climate forcings in Goddard Institute for Space Studies SI2000 simulations, *J. Geophys. Res.*, *107*(D18), 4347, doi:10.1029/2001JD001143.

Horowitz, L. W., J. Liang, G. M. Gardner, and D. J. Jacob (1998), Export of reactive nitrogen from North America during summertime: Sensitivity to hydrocarbon chemistry, *J. Geophys. Res.*, *103*, 13,451–13,476.

Houghton, J. T., B. A. Callander, and S. K. Varney (1993), *Climate Change 1992: The Supplementary Report to the IPCC Scientific Assessment*, 200 pp., Cambridge Univ. Press, New York.

Houghton, J. T., Y. Ding, D. J. Griggs, M. Noguer, P. J. van der Linden, X. Dai, K. Maskell, and C. A. Johnson (2001), *Climate Change 2001: The Scientific Basis, Contribution of Working Group I to the Third Assessment Report of the Intergovernmental Panel on Climate Change*, 881 pp., Cambridge Univ. Press, New York.

Joshi, M., K. Shine, M. Ponater, N. Stuber, R. Sausen, and L. Li (2003), A comparison of climate response to different radiative forcings in three general circulation models: Towards an improved metric of climate change, *Clim. Dyn.*, *20*, 843–854.

Koch, D., D. Jacob, I. Tegen, D. Rind, and M. Chin (1999), Tropospheric sulfur simulations and sulfate direct radiative forcing in the GISS GCM, *J. Geophys. Res.*, *104*, 23,799–23,822.

Lacis, A. A., and V. Oinas (1991), A description of the correlated *k* distribution method for modeling nongray gaseous absorption, thermal emission, and multiple scattering in vertically imhomogeneous atmosphere, *J. Geophys. Res.*, *96*, 9027–9063.

Lenoble, J. (1993), *Atmospheric Radiative Transfer*, 532 pp., A. Deepak, Hampton, Virginia.

Logan, J. A. (1999a), An analysis of ozondesonde data for the lower stratosphere: Recommendations for testing models, *J. Geophys. Res.*, *104*, 16,151–16,170.

Logan, J. A. (1999b), An analysis of ozondesonde data for the troposphere: Recommendations for testing 3-D models and development of a gridded climatology for tropospheric ozone, *J. Geophys. Res.*, *104*, 16,115–16,149.

Manabe, S., and K. Bryan (1985), CO_2-induced change in a coupled ocean-atmosphere model and its paleoclimatic implications, *J. Geophys. Res.*, *90*, 11,689–11,707.

Menon, S., J. Hansen, L. Nazarenko, and Y. Luo (2002), Climate effects of black carbon aerosols in China and India, *Science*, *297*, 2250–2253.

Mickley, L. J., P. P. Murti, D. J. Jacob, J. A. Logan, D. M. Koch, and D. Rind (1999), Radiative forcing from tropospheric ozone calculated with a unified chemistry-climate model, *J. Geophys. Res.*, *104*, 30,153–30,172.

Mickley, L. J., D. J. Jacob, and D. Rind (2001), Uncertainty in preindustrial abundance of tropospheric ozone: Implications for radiative forcing calculations, *J. Geophys. Res.*, *106*, 3389–3399.

Prather, M., and D. Ehhalt (2001), Atmospheric chemistry and greenhouse gases, in *Climate Change 2001: The Scientific Basis. Contribution of Working Group I to the Third Assessment Report of the Intergovernmental Panel on Climate Change*, 881 pp., Cambridge Univ. Press, New York.

Prather, M., et al. (2003), Fresh air in the 21st century?, *Geophys. Res. Lett.*, *30*(2), 1100, doi:10.1029/2002GL016285.

Ramaswamy, V. (2001), Radiative forcing of climate change, in *Climate Change 2001: The Scientific Basis. Contribution of Working Group I to the Third Assessment Report of the Intergovernmental Panel on Climate Change*, 881 pp., Cambridge Univ. Press, New York.

Ramaswamy, V., and M. M. Bowen (1994), Effect of changes in radiatively active species upon the lower stratospheric temperatures, *J. Geophys. Res.*, *99*, 18,909–18,921.

Ramaswamy, V., and M. D. Schwarzkopf (2002), Effects of ozone and well-mixed gases on annual-mean stratospheric temperature trends, *Geophys. Res. Lett.*, *29*(22), 2064, doi:10.1029/2002GL015141.

Rind, D., and J. Lerner (1996), Use of on-line tracers as a diagnostic tool in general circulation model development: 1. Horizontal and vertical transport in the troposphere, *J. Geophys. Res.*, *101*, 12,667–12,683.

Rind, D., J. Lerner, K. Shah, and R. Suozzo (1999), Use of on-line tracers as a diagnostic tool in general circulation model development: 2. Transport between the troposphere and the stratosphere, *J. Geophys. Res.*, *104*, 9123–9139.

Rind, D., J. Lerner, and C. McLinden (2001), Changes of tracer distribution in the doubled CO_2 climate, *J. Geophys. Res.*, *106*, 28,061–29,079.

Rosenfield, J. E., A. R. Douglass, and D. B. Considine (2002), The impact of increasing carbon dioxide on ozone recovery, *J. Geophys. Res.*, *107*(D5), 4049, doi:10.1029/2001JD000824.

Russell, G. L., and D. Rind (1999), Response to CO_2 transient increase in the GISS coupled model: Regional coolings in a warming climate, *Climate, J.*, *12*, 531–539.

Shindell, D. T., and G. Faluvegi (2002), An exploration of ozone changes and their radiative forcing prior to the chlorofluorocarbon era, *Atmos. Chem. Phys.*, *2*, 363–374.

Shindell, D. T., D. Rind, and P. Lonergan (1998), Increased polar stratospheric ozone losses and delayed eventual recovery owing to increasing greenhouse-gas concentrations, *Nature*, *392*, 589–592.

Shindell, D. T., G. A. Schmidt, R. L. Miller, and D. Rind (2001a), Northern Hemisphere winter climate response to greenhouse gas, ozone, solar, and volcanic forcing, *J. Geophys. Res.*, *106*, 7193–7210.

Shindell, D. T., G. A. Schmidt, M. E. Mann, D. Rind, and A. Waple (2001b), Solar forcing of regional climate change during the Maunder Minimum, *Science*, *294*, 2149–2152.

Stuber, N., M. Ponater, and R. Sausen (2001), Is the climate sensitivity to ozone perturbations enhanced by stratospheric water vapor feedback?, *Geophys. Res. Lett.*, *28*, 2887–2890.

Wang, Y., and D. J. Jacob (1998), Anthropogenic forcing on tropospheric ozone and OH since preindustrial times, *J. Geophys. Res.*, *103*, 31,123–31,135.

Wang, Y., D. J. Jacob, and J. A. Logan (1998), Global simulation of tropospheric O_3-NO_x-hydrocarbon chemistry, 1. Model formulation, *J. Geophys. Res.*, *103*, 10,713–10,725.

Williams, K. D., A. Jones, D. L. Roberts, C. A. Senior, and M. J. Woodage (2001), The response of the climate system to the indirect effects of anthropogenic sulfate aerosol, *Clim. Dyn.*, *17*, 845–856.

B. D. Field, D. J. Jacob, and L. J. Mickley, Division of Engineering and Applied Sciences, Harvard University, 29 Oxford Street, Cambridge, MA 02138, USA. (bdf@io.harvard.edu; djj@io.harvard.edu; ljm@io.harvard.edu)

D. Rind, Goddard Institute for Space Studies, Columbia University, 2880 Broadway, New York, NY 10025, USA. (drind@giss.nasa.gov)

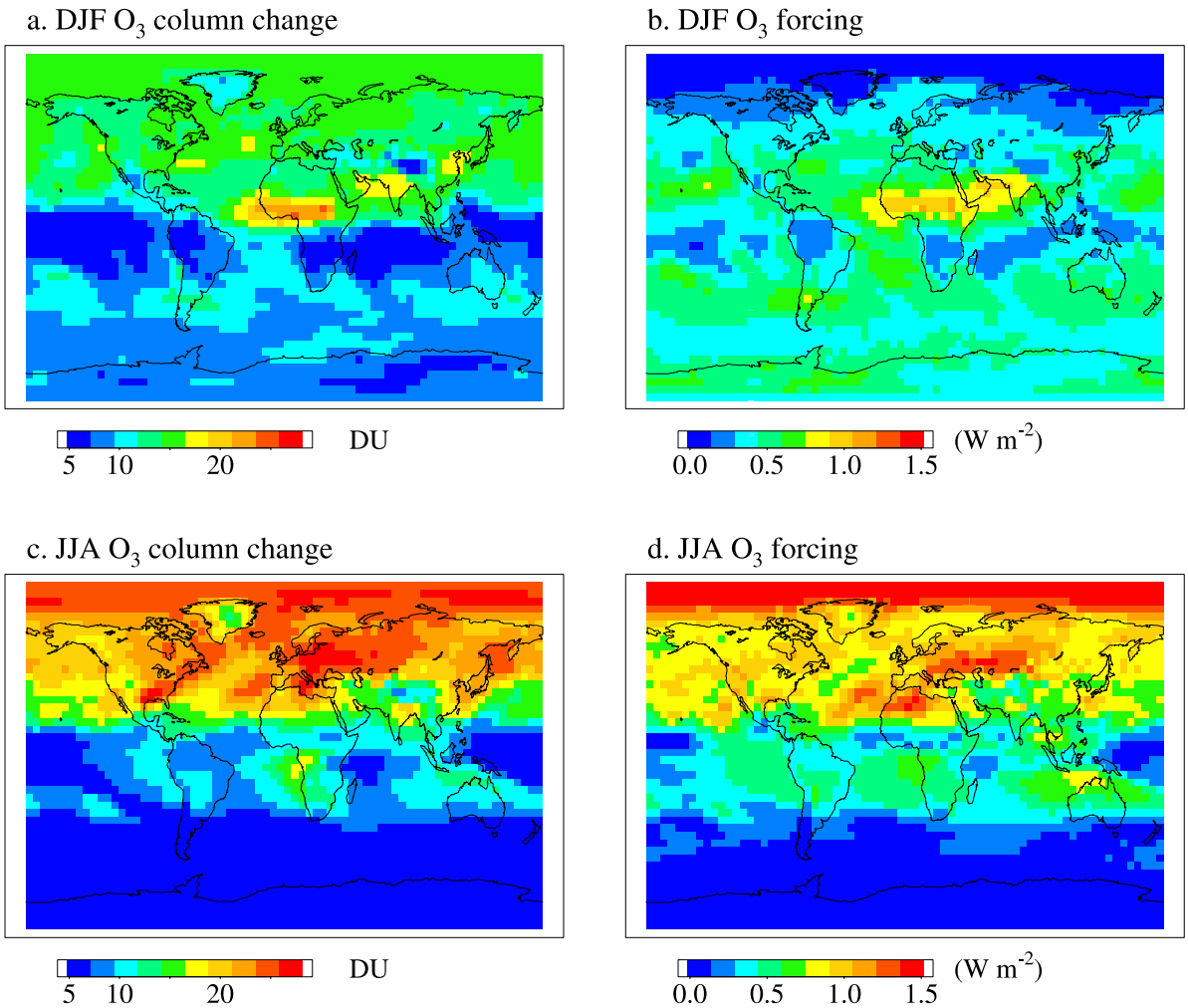

Figure 2. Calculated column change of tropospheric ozone since preindustrial times in Dobson units (DU) and the corresponding instantaneous radiative forcings at the tropopause in W m^{-2} for DJF (a, b) and JJA (c, d).

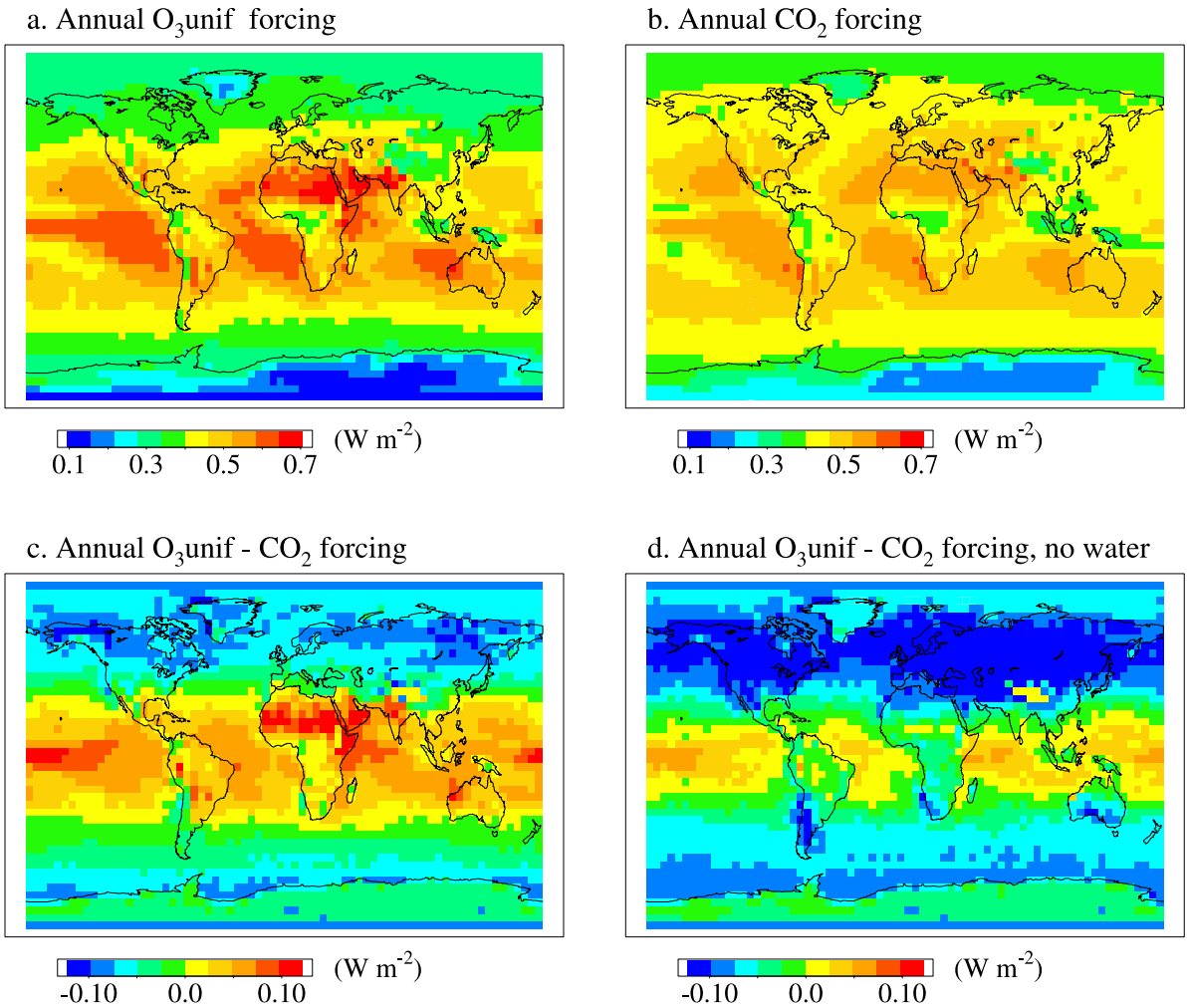

Figure 3. Calculated, annual mean, instantaneous forcing at the tropopause due to (a) an 18-ppb increase in tropospheric ozone applied uniformly throughout the troposphere to preindustrial ozone and (b) a 25-ppm increase in CO_2. Figure 3c shows the difference between these two forcings; Figure 3d shows the difference when the interference due to water vapor is excluded from the calculation.

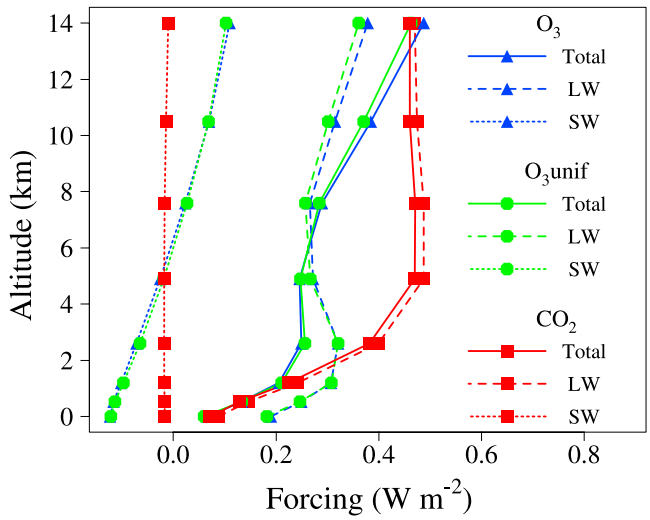

Figure 4. Vertical distribution of radiative forcing for (a) the calculated ozone increase from preindustrial times to the present-day (blue curves, triangles), (b) an equivalent 18-ppb increase of ozone (green curves, circles), and (c) a 25-ppm CO_2 increase (red curves, squares). The dashed curves denote the longwave forcings; the dotted curves, the shortwave forcings; and the solid curves, the total (longwave + shortwave) forcings. Values are annual global means. The forcings represent values at the edges of the model layers, beginning at the bottom with the forcing at the Earth's surface.

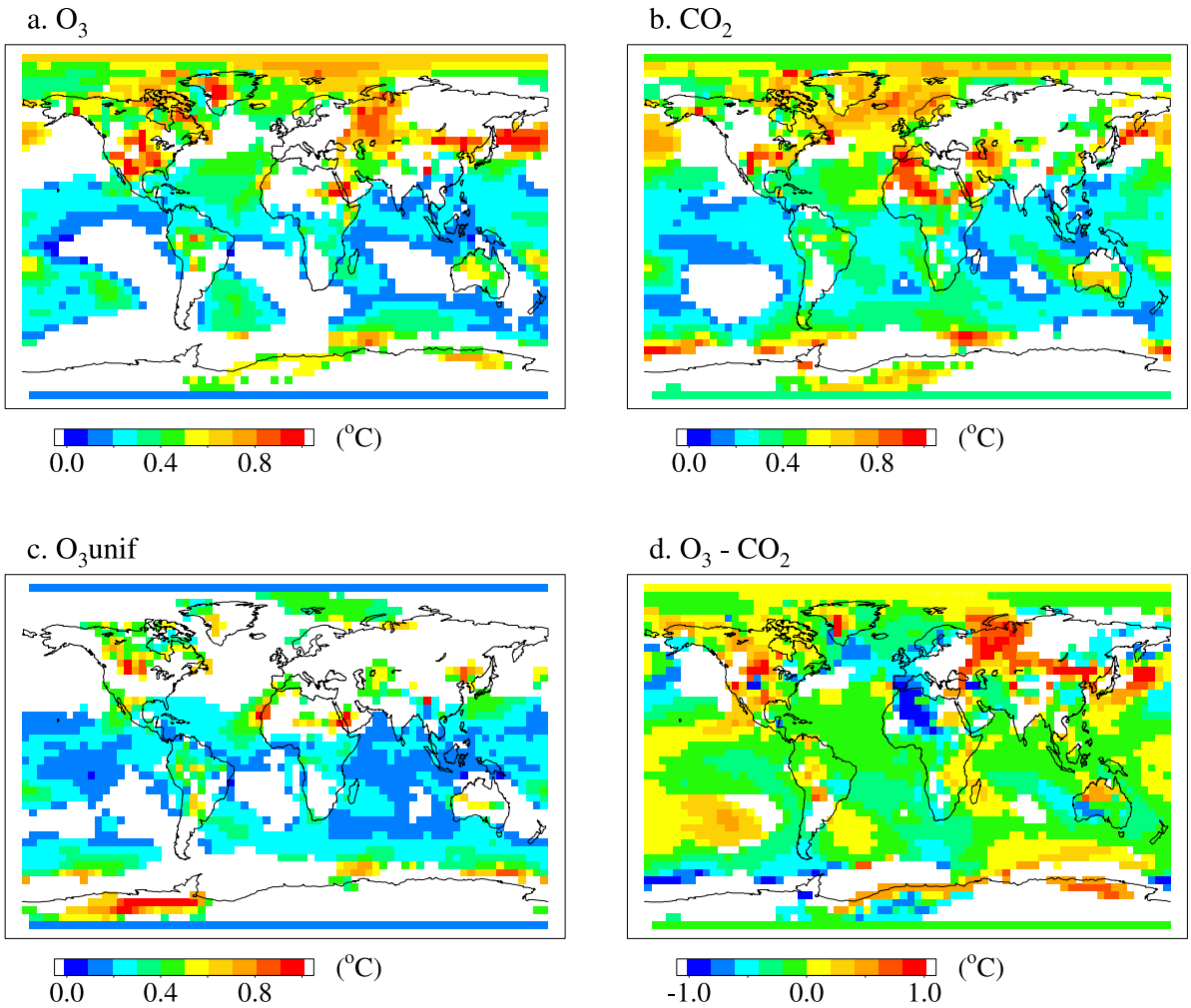

Figure 10. JJA surface temperature response to (a) the calculated increase in ozone, (b) the 25-ppm increase in CO_2, and (c) the 18-ppb uniform change in ozone. Figure 10d shows the difference in surface temperature response between the calculated ozone case and the CO_2 case. White areas indicate insignificant values at the 95% level as determined by the student's two sample t-test. In calculating differences in Figure 10d, insignificant values were assumed to be zero.

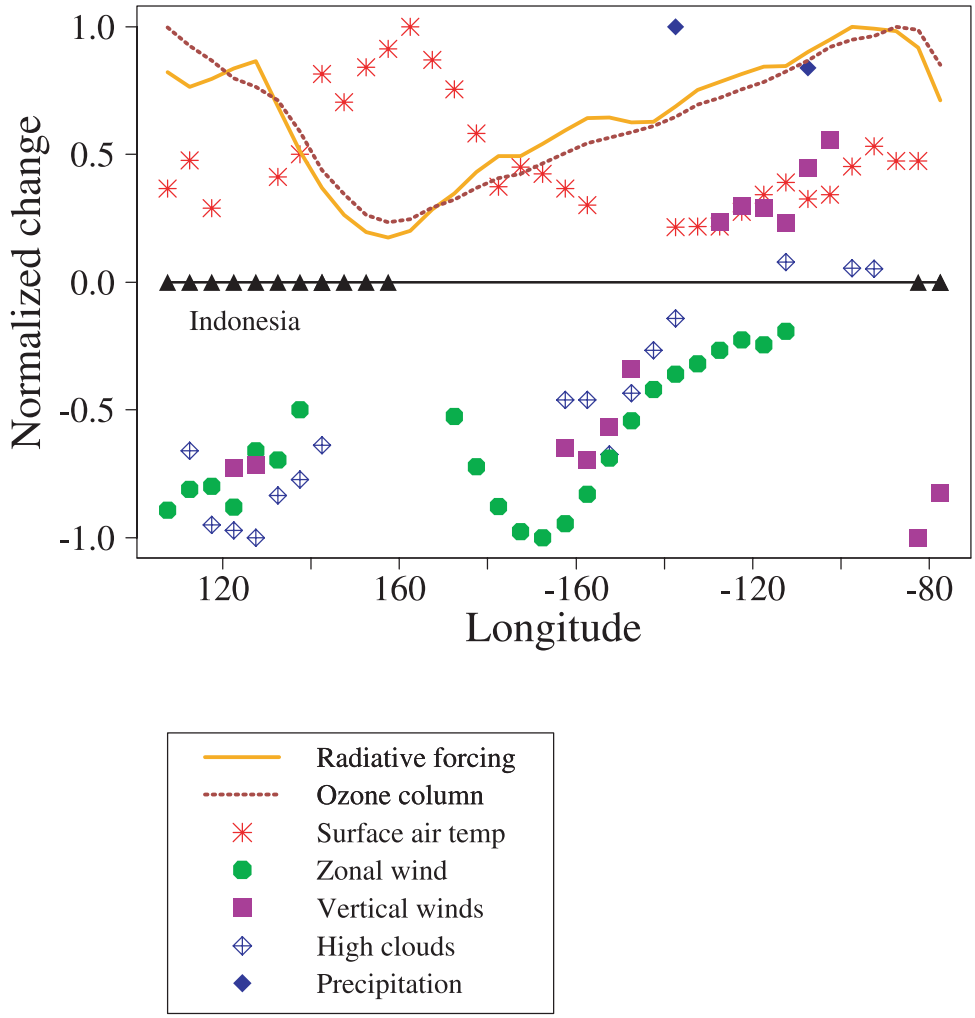

Figure 11. Normalized meteorological changes due to the calculated ozone increase over the equatorial Pacific since preindustrial times (mainly biomass burning), as a function of longitude. Variables are averaged over the 2–6 S latitude band and normalized to the maximum absolute values of each change. The solid gold curve denotes the ozone column change between the surface and the tropopause and the dotted brown curve shows the corresponding radiative forcing. The symbols show the changes in surface air temperature, surface zonal wind, vertical winds, high cloud cover, and precipitation. Only significant changes are shown. The black triangles denote longitude bands that contain land.